Estimation of the spatiotemporal dynamic of snow water equivalent at mountain range scale under data scarcity

Antonio-Juan Collados-Lara[1] *, David Pulido-Velazquez[1], Eulogio Pardo-Igúzquiza[2], Esteban Alonso-González[3]

1 Instituto Geológico y Minero de España, Urb. Alcázar del Genil, 4. Edificio Zulema Bajo, 18006, Granada (Spain). E-mails: ajcollados@gmail.com; d.pulido@igme.es

2 Instituto Geológico y Minero de España, Ríos Rosas, 23, 28003 Madrid (Spain). E-mail: e.pardo@igme.es

3 Instituto Pirenaico de Ecología, Consejo Superior de Investigaciones Científicas (CSIC), 50059 Zaragoza (Spain). E-mails: e.alonso@ipe.csic.es

* Corresponding Author

Abstract

The snow dynamics in alpine systems play a significant role in the hydrosphere, biosphere, and anthroposphere interfaces of these regions. The storage of water resources as snow is essential for ecosystems, human consumption, tourism, and hydropower in many areas. However, snow data are usually scarce due to poor accessibility, difficulties to maintain monitoring system under harsh climatic conditions and limited economic funds. Most of the scientific studies aimed to quantify water stored as snow are carried out at small or medium spatial scales, but few analyses are done for the whole mountain ranges. The main goal of this work is to propose a general parsimonious methodology to estimate snow water equivalent under data scarcity for the Sierra Nevada mountain range (Spain). The methodology is easily transferable to any other study areas. It combines a dynamic regression approach of snow depth from punctual data, snow cover area data from the MODIS satellite and simulations of snow density from a coupled mass and energy balance model. The regression model includes two kinds of explanatory variables (steady and non-steady) to assess the snow depth dynamics. The dynamic of the snow density in the mountain range has been obtained using a physically based simulation driven by climate model data for the Iberian Peninsula. These three variables (snow depth, snow cover area and snow density) have been used to obtain spatially distributed series of snow water equivalent for the whole mountain range. The proposed solution allows to study the snow water equivalent distribution, duration of the snow cover and number of accumulation and melting days for different snow seasons. The mean accumulated snow water equivalent per season in the historical period is 330 Hm3 and the maximum of 480 Hm3, which is a significant amount of resources in an area characterized by limited water availability.

Keywords: water resources, snow depth, snow cover area, snow density, alpine systems, Sierra Nevada (Spain)

List of abbreviations

SWE	Snow water equivalent
SD	Snow depth
SCA	Snow cover area
ASCA	Accumulated snow cover area
SDEN	Snow density
P	Precipitation

1. Introduction

Water stored in snowpack is essential for understanding the amount of water and its seasonal distribution in alpine regions and their surrounding areas (Zappa et al., 2019). It represents a natural storage system that, in general, accumulates snow during winter and releases water during the summer period. The assessment of the spatiotemporal distribution of these resources is a topic of interest for scientists, water policy managers and society (Viviroli et al., 2011; Sturm et al., 2017). Snow water equivalent (SWE), which is the amount of water contained within the snowpack, can be assessed as the product of three variables: snow depth (SD), snow cover area (SCA), and snow density (SDEN). The assessment of the spatiotemporal variability of SWE is a key issue to plan and management human water consumption and renewable energy production, such as hydropower in many mountains areas around the world (Mankin et al., 2015; Kuriqi et al., 2019). The assessment of snow variables is a non-trivial problem and requires snow measurements (e.g. Salomonson and Appel, 2004; López-Moreno and Nogués-Bravo, 2006; López-Moreno et al., 2013, Bormann et al., 2013).

Nevertheless, snow data in most of alpine regions are usually scarce. The poor accessibility to mountains ranges due to the high elevation, rough topography, climatology, and the presence of ice and snow makes the monitoring of snow in alpine regions complicated (Zhang et al., 2014; Ren et al., 2018). Sometimes it can be overcomed by using automatic weather stations (Fassnacht et al., 2017) or airborne LIDAR (Light Detection and Ranging) (Harpold et al., 2014; Skaugen and Melvold, 2019), but, such options are expensive to implement making them unfeasible in many areas.

Another alternative is the use of SWE products derived from satellite microwave radiometer-based measurements. For example, the Global Snow Monitoring for Climate Research (GlobSnow) product of the European Space Agency (ESA) (Luojus et al., 2010; Metsämäki et al, 2015) provides SWE retrievals of 25-km resolution for the Northern Hemisphere; The Microwave Surface and Precipitation Products System (MSPPS) product of the National Oceanic and Atmospheric Administration (NOAA) (Ferraro et al., 2002; Ferraro et al., 2005) provides global 16-km resolution SWE retrievals. However, the spatial resolution of these products cannot be adequate for some distributed hydrological applications where snow accumulation and melting processes are approached in small catchments or mountain range studied (Pardo-Iguzquiza et al., 2017; Jimeno-Saez et al., 2020). Finer spatial resolutions are also recommended due to the complex topography of alpine regions (Dong et al., 2005), otherwise, these products should be evaluated and combined with high-resolution digital elevation information such as the Shuttle Radar Topography Mission (SRTM) (Molotch et al., 2005).

In cases where finer spatial resolutions are needed and a relative abundance of snow and meteorological information are available it is possible to have good approximations of SWE by using physically based simulations. They can be applied directly to SWE (Langlois et al., 2009) or to the secondary variables [SD (Liston and Elder, 2006); SCA (Zeinivand and De Smedt, 2009); SDEN (Brun et al., 2013)].

However, when limited data are available geostatistical techniques can be useful to interpolate the SWE (Carroll and Cressie, 1996) or the variables that define it. SCA has been analyzed using regression techniques (Richer et al., 2013; Mir et al., 2015). In the same way, SD and SDEN can be estimated using geostatistical techniques (López-Moreno and Nogués-Bravo, 2006, Collados-Lara et al., 2017; Prusova et al., 2012). Geostatistical techniques are useful to define the optimal location of snow poles too (Collados-Lara et al., 2020). The outputs of these techniques can be constrained by the SCA information derived from satellites. In the case of SCA, satellite products provide good approximations at finer scales [e.g. MODIS at 500-m resolution (Hall et al., 2002); LANDSAT at 30-m resolution (Girona-Mata et al., 2019); SENTINEL at 10-m resolution (Gascoin et al., 2018); PLEIADES at 0.5-m resolution (Shaw et al., 2020)] but the presence of clouds or the temporal resolution higher than daily (e.g. LANDSAT) make necessary techniques for gap filling the daily series.

On the other hand mixed approaches that combine SD information using geostatistical methods or observation techniques such as airborne LIDAR and physical simulations of SDEN (with a lower range of uncertainty than SD) have been employed satisfactorily to estimate SWE (e.g. Painter et al., 2016).

The main objectives of this work are: (1) to propose a novel approach to estimate daily spatial distribution of SWE at mountain range scale and (2) to assess the spatiotemporal dynamics of SWE in the Sierra Mountain Range (Southern Spain). The proposed methodology is a general approach specially indicated when the snow information is limited to sparse punctual and temporally discontinuous information on snow depth. An integrated modelling approach is proposed by combining a dynamic regression approach of SD, SCA data from remote sensing and simulations of SDEN from a coupled mass and an energy balance model. The SD model has been derived from the model developed by Collados-Lara et al. (2017) and the density simulations were performed by using the approach proposed by Alonso-González et al. (2018).Results from the proposed methodology permitted analyzing the SWE distribution, duration of the snow cover and, number of accumulation and melting days during the period 2000-2014 for the case study.

The rest of the manuscript is organized as follows: The study area (Sierra Nevada Mountain range) is described in Section 2, the employed data for the case study are included in Section 3.1 and the proposed methodology to estimate SWE is described in Section 3.2. Section 4 presents the results, and their discussion is included in Section 5. Lastly, Section 6 presents the main conclusions of this research.

2. Study area

The Sierra Nevada mountain range is located in southern Spain (see Figure 1). It has an extension of around 80 km in the west-east direction and between 15 and 30 km in the north-south direction. The highest peak of the Iberian Peninsula (Mulhacén Peak, 3478.6 m a.s.l.) is located in Sierra Nevada. It enjoys a high-mountain Mediterranean climate (Collados-Lara et al., 2018). Summers are relatively dry and the winters are wetter with a high spatial and inter annual variability of precipitation (P) (Herrero et al., 2011). In Sierra Nevada, from November to April the majority of P falls as snow, which is very important for the region from the tourism (it is the southernmost ski station in Europe), environmental and water resources perspective. It is also included in different figures of protection (Natural and National Park and Biosphere Reserve) that aim a good state of conservation of the environmental resources. The snowfall is essential to the availability of water resources in the Sierra Nevada catchments and the city of Granada (Herrero et al 2009). The study of the snow dynamics is a key issue for the region.

3. Data and Methods

3.1 Data

The proposed methodology (explained in section 3.2) requires snow, climatic, and orographic information. For the case study we used SD information from 23 snow poles (see Figure 1) (Collados-Lara et al., 2020) from 10 surveys provided by the Spanish Ministry of Agriculture Food and Environment (within the framework of the ERHIN program (Assessment of Water Resources from Snow Accumulation). We also included daily SD data elaborated by Pimentel et al. (2017) for the period 2009-11-15 to 2013-05-31 in Refugio Poqueira. They employed terrestrial photography over a plot study area to define local snow depth. The distribution of the SD data employed is this work has a positive skew (mean 56.6 and median 34.1 cm) and the majority of the data (84%) are lower than 100 cm. The minimum and maximum values are respectively 0 and 450 cm. This information has been used to calibrate the SD regression models. We also used fractional SCA data from the MODIS satellite. We employed the MODIS/Terra Snow Cover Daily Global 500 m Grid (Data Set ID: MOD10A1), which has a spatial resolution of approximately 460 m for the latitude of the study area and a temporal resolution of 1 day. We have approximated the SCA in cloudy dates without MODIS information by linear interpolation between the nearest previous and subsequent cloudless days. The SCA dynamic in Sierra Nevada has been previously assessed in other research papers (Pardo-Igúzquiza et al., 2017; Collados-Lara et al., 2019). These data have been employed to calculate the non-steady indices of SCA and for the final calculation of SWE. On the other hand, SDEN data were obtained by Alonso-González et al. (2018), further details in section 3.2. These data have been employed to estimate

SWE too. The elevation data was obtained from a digital elevation model of 5-meter resolution elaborated by Spanish National Geographic Institute. This elevation model was used to estimate the spatial explanatory variables. P and temperature data were employed to calculate additional non-steady indices. They were obtained from the Spain02 v04 project (Herrera et al. 2016). It includes daily estimates of P and temperature for Spain in the period 1971-2010 with a spatial resolution of 12.5 km.

These data have been used to obtain SD and SWE in the area of interest which has been divided into a finite number of cells using the spatial resolution of the MODIS product. SD obtained from the dynamic regression model and SCA from MODIS uses the same spatial support (grid cell of about 460 x 460 m) and SDEN data are distributed in grid cells of 10 x 10 km. The daily density used for each 460 x 460 m pixel has been selected taking into account its location with respect the 10 x 10 km grid and the range of elevation where the pixel is located. Note that the SDEN data are distributed by cells and ranges of elevations. With respect elevation, mean values were calculated for the calculation grid.

3.2. Estimation of distributed snow depth, density, and water equivalent

The proposed methodology (summarized in Figure 2) aims to assess the SWE in a mountain range where very limited snow depth (23 observation sites in the whole range measured only once or twice every year) and density information is available. Two different models are applied in a sequential way: a dynamic regression model to estimate SD, and a physically based model driven by downscaled reanalysis data to estimate SDEN. The SWE is obtained by combining this information with SCA values obtained from satellite information.

Three non-steady regression models have been considered to simulate the SD dynamics by using continuous steady (they do not vary in time) and non-steady variables (they vary in time). Their formulation was derived from an optimal steady regression model that produced the best approximation to the historical SD observations (Collados-Lara et al., 2017):

$$Y = \beta_0 + \beta_1 x_i + \beta_2 x_j + \beta_3 x_l x_k \qquad (1)$$

where Y is the variable to be estimated (in this case SD), $\{x_i, x_j, x_l, x_k\}$ are the steady explanatory variables and/or their mathematical transformations , and $\{\beta_0, \beta_1, \beta_2, \beta_3\}$ are unknown parameters estimated from experimental data. The sub-index i, j, l, k indicates that the variables and/or their transformations can be different.

Three new solutions have been defined from this regression model by using different formulations where non-steady variables and/or their transformations $\{t_n, t_o, t_p\}$ have been included (see Equations 2−4). The sub-index n, o, p indicates that the variables and/or their transformations can be different. Note that $\{t_n, t_o, t_p\}$ can also take the value 1 in cases in which the non-steady variables would not improve the accuracy of the results.

$$Y_1 = \beta_0 + (\beta_1 x_i + \beta_2 x_j + \beta_3 x_\ell x_k) t_n \qquad (2)$$

$$Y_2 = (\beta_0 + \beta_1 x_i + \beta_2 x_j + \beta_3 x_\ell x_k) t_n \qquad (3)$$

$$Y_3 = \beta_0 + \beta_1 x_i t_n + \beta_2 x_j t_o + \beta_3 x_\ell x_k t_p \qquad (4)$$

Note that model 1 is a particular case of model 3

Nine steady explanatory variables (elevation, slope, longitude, latitude, eastness, northness, maximum upwind slope, radiation, curvature) (Fassnacht et al., 2013; Collados-Lara et al., 2017) and its transformations (square, root square, inverse and logarithm) have been considered in this study to explain the spatial variability of SD. With respect to the temporal variability, two non-steady explanatory variables have been considered: the SCA and the solid P accumulated in a temporal window. In this study we have tested two different assumptions to identify when the P is solid: mean temperature < 0ºC, and minimum temperature < 0ºC. Two options have been considered to define the temporal windows to accumulate the non-steady variables:

$$t^1_{v,\zeta} = \frac{1}{2\zeta+1} \sum_{v-\zeta}^{v+\zeta} t_w \qquad (5)$$

$$t^2_{v,\zeta} = \frac{1}{\zeta+1} \sum_{v-\zeta}^{v} t_w \qquad (6)$$

where $t^1_{v,\zeta}$ is the accumulation of the variable t_w in the time v considering the temporal window $[v-\zeta, v+\zeta]$ and $t^2_{v,\zeta}$ is the accumulation of the variable t_w in the time v considering the temporal window $[v-\zeta, v]$.

We have also considered the square, root square, inverse and logarithm transformations for the non-steady variables. In the case of the non-steady explanatory variables the neutral element of multiplication has been considered too. It intends to consider the non-steady variables only when they improve the accuracy of the model.

In order to identify the best regression models, we assessed the goodness of fit for all the possible combinations of model structures (the three formulations defined in Equations 2−4) and the 65 combinations of variables (including steady and non-steady explanatory variables and its transformations and accumulations). The parameters of the three considered structures (Equations 1-3) have been calibrated by solving an optimization problem by applying maximum likelihood normal regression. Different indices were used to assess the goodness of fit: the coefficient of determination (R^2), the adjusted R^2 (R^2_{adj}), the negative of the logarithm of likelihood function (NLLF), the Akaike information criterion (AIC), the Bayesian information criterion (BIC), and the Kashyap information criterion (KIC).

The selected model allowed us to estimate daily SD in each pixel in our case study. In order to reduce the uncertainty in the estimation, SCA data are used to define the pixels that are covered by snow. In this study we have considered a pixel covered by snow if its SCA is higher than 50%.

The daily dynamics of the SDEN in the mountain range has been taken from the simulation with a physically based model with a coarse resolution. Thus, an energy mass and energy snowpack model (Factorial Snow Model 1.0, FSM) (Essery, 2015) driven by the regional atmospheric model the Weather Research and Forecasting (WRF) (Skamarock et al., 2008) was used following the methodology proposed by Alonso-González et al. (2018). They used a pre-existing WRF simulation as meteorological forcing of FSM. The WRF simulation had a 10km cell size with a 3h time step covering the whole Iberian Peninsula. The boundary and initial conditions of WRF were provided by the ERA-Interim global reanalyses and the WRF parametrization was tested using observations over the whole Iberian Peninsula. The complete description of the WRF configuration can be found in García-Valdecasas Ojeda et al. (2017). Then, the WRF outputs where reprojected to different elevation bands at 100m steps (from 1500 to 2900 m a.s.l.) to simulate the snowpack at all the elevations inside each WRF cell using an array of psychrometric and radiative formulae and lapse rates. FSM was setup in its most physically based configuration. Thus albedo decrease as snow aged, and increases with new snowfalls. The compaction rate was calculated from the thermal metamorphism and overburden (Verseghy, 1991), allowing the retention and refreezing of water in the snowpack. Finally the turbulent exchange coefficient was corrected based on the bulk Richardson number and the thermal conductivity was calculated based on snow density. The snow series were validated using data from gapfilled MODIS satellite sensor (Gascoin et al., 2015) and ground observations. A complete description of the methodology and its validation using in situ snow measurements and MODIS SCA can be found in Alonso-González et al. (2018).

This information has been incorporated to our dynamic model of SD along with SCA from satellite to calculate SWE. The spatially distributed daily series of SWE allowed us to characterize the snow dynamics of the case study for different snow seasons using different statistics: distribution of SWE by elevation ranges, duration of the snow season, number of accumulation and melting days.

4. Results

The dynamic regression models of SD (Eq. 2, 3, and 4) have been calibrated for the whole Sierra Nevada Mountain range and compared in terms of different indices (see section 3.2.). Nine steady explanatory variables and its transformations (see Figure 2) have been considered combining them with non-steady explanatory variables defined as (1) the accumulated SCA and (2) the accumulated P within a period. The different models studied are showed in Table 1. They differ in the model structures (Equations 2-4), non-steady variables (SCA and P accumulated when mean or minimum temperature is below zero), and options of accumulations (Equations 5 and 6).

Figure 3 shows the accuracy of the different models using the accumulated SCA within different temporal windows of accumulation (ζ from 0 to 330 days). In general, better approximations are provided by the model structure 3 (see Equation 4). We have also tested a model whose non-steady variable is the accumulated P when the temperature is above a threshold. Two different thresholds have been tested: mean temperature below 0 ºC, and minimum temperature below 0 °C. The R^2 values from these experiments considering different temporal windows of accumulation (ζ from 0 to 330 days) are showed in Figure 4. In the approach with SCA the maximum R^2 obtained is 0.64 for the model m3_v2_SCA and the optimal temporal accumulation $t_{v,\zeta}^{2}$ with ζ = 25 days. Using the temporal accumulation $t_{v,\zeta}^{1}$, ζ = 30, and model m3_v2_SCA similar accuracy is obtained (R^2 0.63). When P is used, the maximum R^2 obtained is 0.61 for the model m3_v2_P(Tmin), for the temporal accumulation $t_{v,\zeta}^{2}$ with ζ = 120 days, being the temperature threshold set by using the minimum temperature. In both approaches (using SCA or P), the minimum R^2 obtained is 0.59, which correspond to the models that includes only steady variables. For some temporal windows of accumulation (ζ) the best model is the steady one. Note that the steady option has been also included between the models tested. The value of the rest of the indices of goodness of fit calculated for these models is included in Table 2.

The explanatory variables and their relationship with the parameters for the steady model and the best non-steady models for SCA and P (m3_v2_SCA with $\boldsymbol{\zeta}$ = 25 or 30 and m3_v2_P(Tmin) with $\boldsymbol{\zeta}$ =120) are showed in Equations 7, 8, and 9 respectively.

$$SD = \beta_0 + \beta_1 E + \beta_2 S^2 + \beta_3 M^2 C^2 \qquad (7)$$

$$SD = \beta_0 + \beta_1 \frac{E}{SCA} + \beta_2 \frac{E^2}{SCA} + \beta_3 S^2 \sqrt{C} \qquad (8)$$

$$SD = \beta_0 + \beta_1 \frac{\sqrt{P}}{S} + \beta_2 E^2 + \beta_3 S^2 \sqrt{C} \qquad (9)$$

Where SD is snow depth, E is elevation, S is slope, M is maximum upwind slope, C is curvature, SCA is snow cover area, P is precipitation, and $\{\beta_0, \beta_1, \beta_2, \beta_3\}$ are estimated parameters.

Note that the model structure of Equation 8 is obtained for both m3_v2_SCA using ζ = 25 and ζ = 30. Both options present similar indices of goodness of fit (see Table 2). The mean SD obtained for the mountain range vs. accumulated SCA (ASCA) is represented for these models in Figure 5a and 5b respectively. Note that, for low values of ASCA, high values of mean SD with low correlations with ASCA (especially for m3_v2_SCA with ζ = 25) (see Figure 5d) are obtained. It is due to there is not SD observations for high ASCA values, and, therefore, a dynamic coefficient to improve the estimation in this range could not be obtained. For this reason, we propose a piecewise function in which the steady model (Equation 7) is employed for ASCA lower than or equal to 10% and the model m3_v1_SCA with ζ = 30 for ASCA higher than 10%. This combination has been called m3_v1_SCA*. The mean SD obtained for the mountain range vs. ASCA for m3_v1_SCA* is showed in Figure 5c and the correlation coefficient of the relationship between mean SD and ASC for different thresholds of ASCA in Figure 5d. This piecewise function model provides good results for all the ranges of ASCA and has been employed for the subsequent assessment of SD and SWE.

Figure 6a shows the spatial distribution of the mean SD in the whole Sierra Nevada mountain range for the snow season (October to May). We obtained values of mean SD higher than zero for elevation above1400 m.a.s.l. being the mean value higher than 35 cm for elevation higher than 2200 m.a.s.l. The standard deviation of SD is showed in Figure 6b. Higher standard deviation is obtained for higher elevation. Note that higher SD is obtained for higher elevation and during the summer SD is zero for the whole mountain range. The intra- and inter-season variability can be observed in Figure 7a, where temporal series of the estimated mean SD within the historical period 2000-2014. An example of the significant differences between seasons is shown in Figure 7b, where the mean SD for the seasons 2007-2008 and 2008-2009 is represented.

Distributed density in a grid of 10 x 10 km has been estimated for Sierra Nevada Mountain by using the simulations of SD and SWE obtained by Alonso-González et al. (2018) as explained in section 3.2. The mean daily density for the mountain range is showed in Figure 8a for the different elevation ranges considered. Unlike mean SD dynamic, which experiment the maximum values around the half of the snow season (see Figures 7a and 7b), mean SDEN show the maximum values at the end of the snow season for all the elevation ranges (see Figure 8b). Mean SDEN varies from around 100 kg m^{-3} in October to 500 kg m^{-3} in May without significant differences between elevation ranges.

The distributed values of SDEN have been combined with the SD model and SCA data to estimate SWE. The spatial distribution of the mean SWE for the whole mountain range during the snow season is showed in Figure 9a. In accordance with the SD results, we obtain values of mean SWE higher than zero for elevation above1400 m.a.s.l. The mean value of SWE is higher than 9 cm when the elevation is above 2200 m.a.s.l. The spatial (see Figure 9b) and temporal (inter and intra-season) (see Figure 10) variability of SWE is high, as was also observed for SD. However, the maximum values of SWE are not always localized in the middle of the season, due to the influence of the SDEN which is higher at the end of the season. If we focus on the mean year at monthly scale (Figure 11) the maximum mean value of SWE for the mountain range is reached in March and it is around of 60 Hm^3 but the global maximum is around 90 Hm^3 and it was reached in February 2009. For the case study, one season (2011-2012) has the maximum monthly mean SWE in November, five seasons (2003-2004, 2005-2006, 2007-2008, 2008-2009, and 2012-2013) in February, five seasons (2000-2001, 2001-2002, 2004-2005, 2006-2007, and 2013-2014) in March, and three seasons (2002-2003, 2009-2010, and 2010-2011) in April. Figure 11 shows that the accumulation of snow in Sierra Nevada Mountain occurs from November to March while the majority of snow melts appear in April. We have also studied the variability of the SWE in different elevation ranges (see Figure 12). In absolute terms (SWE equivalent measured in volume) the majority of water related to snow is accumulated in the range of elevation from 2700 to 3100 m.a.s.l. (see Figure 12a). However the SWE measured in length (without considering the area covered by snow) systematically increases from lower to higher elevation (see Figure 12b). The maximum mean monthly value of SWE is around 96 cm and it is obtained for the elevation range 3300-3500 m.a.s.l.

The temporal dynamic of SWE in Sierra Nevada (Figure 10a) shows different periods of accumulation and melting during the snow seasons. The total water resources coming from snow can be estimated by integrating the SWE values along the snow season (Figure 13a). All seasons show more or less similar slope in the accumulation of snow. Nevertheless, we observe different starting of seasons which, beside the differences in the accumulation slope, produces different total accumulated SWE. Seasons 2001-2002 and 2008-2009 show the most significant accumulated SWE (higher than 400 Hm^3), which are associated to higher slopes of accumulated SWE and early starting of the snow seasons. The length of the snow period, number of snow accumulation and melting days, and total SWE accumulated for each snow season is showed in Figure 13b.

5. Discussion

In this study we have generated distributed daily data of SWE for the whole Sierra Nevada Mountain using one or two SD measurements per snow season taken from 2000 to 2014 by the ERHIN program in only 23 points. This information very limited compared to other mountain regions of the world (e.g. the information provided by Natural Resources Conservation Service (NRCS) for the USA Mountains through the SNOTEL system (Natural Resources Conservation Service, 2016) but it is very useful for monitoring the snow dynamic of the region. The limited information available in some mountain ranges makes necessary to develop specific methodologies for estimating SWE as presented here. The presence of snow in alpine systems influences on the dynamic within different interfaces (hydrosphere, biosphere, and anthroposphere) of the regions where these systems are located. The reduction of snow resources will change pattern of the streamflow hydrograph [e.g. due to climate change (Collados-Lara et al., 2019)] and may affect significantly toin this work ecosystems (Löffler, 2007), human water consumption (Mankin et al., 2015), tourism (Soboll, A., Dingeldey, A. 2012), and hydropower (Kuriqi et al., 2019) in alpine areas.

We used an integrated modelling approach by combining a dynamic regression approach of SD, SCA data from remote sensing and simulations of SDEN from a coupled mass and an energy balance model. The combination of statistical and physically based methodologies has been usually employed satisfactorily in geosciences to simulate land surface processes [e.g. streamflow (Rosenberg et al., 2011); SWE (Bavera et al., 2014)]. In this case, the regression model to estimate SD is calibrated with a few distributed observations associated to snow poles. It also has lower computational requirements than completely physically based approaches.

The estimation of snow variables by using regression or interpolation models has been widely applied in previous works.. For example, López-Moreno and Nogués-Bravo (2006) evaluated a number of interpolation methods for mapping snow depth; Mir et al. (2015) used a simple linear regression to analyse the relationship between the variation in SCA and snowfall; Fassnacht et al., 2003 evaluated inverse weighted distance and regression techniques to estimate SWE. In this work we use a dynamic regression model to estimate SD, in which hydrological non-steady variables (P and SCA) are used as explanatory variables of SD. It allows to propagate to the snowpack the impacts of potential climate change on SCA or P (Collados-Lara et al., 2019).

The proposed methodology has proven to be an efficient approach to estimate SWE for the whole mountain range with the limited information available. Despite Sierra Nevada Mountain (Spain) is a small mountain range compared to others around the world, such as the Pyrenees (Sanmiguel-Vallelado et al., 2017), Alps (Marty et al., 2017), Rocky Mountains (Fassnacht et al., 2018) and Sierra Nevada (USA, Wrzesien et al., 2017) the methodology can be applied to those larger mountain ranges too.

We estimated daily SD and SWE spatially distributed at 460-m resolution. Previous works estimated these variables for the whole mountain range of Sierra Nevada but the spatial and temporal resolution were limited [e.g. Collados-Lara et al. (2017) estimated SD and a first approximation of SWE (considering a constant value of density) at 460-m resolution for eleven days; Alonso-González et al. (2018) estimated daily SD and SWE at 10-km spatial resolution (around 20 pixels in Sierra Nevada)].

The snow of the Sierra Nevada mountain range plays a significant role in the water resources (among others) of the region. It constitutes a natural storage system of great value in semiarid zones located around the mountain. The mean total SWE accumulated in a snow season in the period 2000-2014 is around 330 Hm^3 and the maximum around to 480 Hm^3. Note that, the sum of the maximum capacity of the two reservoirs (Canales and Quentar) that supply water to the Granada city is around 84 Hm^3 (Delgado-Ramos and Hervás-Gámez, 2018).

5.1. Hypotheses, limitations and future works

We presented a general method to estimate the spatiotemporal dynamic of SWE at mountain range that could be applied to any case study, even when the available data are scarce. Although it has proven to be an efficient approach to estimate SWE, we wanted to highlight some hypothesis assumed and the limitations of this application:

- SWE is calculated by integrating estimated SD, SCA, and SDEN. While SD and SCA have the same spatial support (460-m resolution), SDEN is associated to a different spatial support (10-km resolution). For the assessment of SWE at 460-m resolution, we matched each 460-m pixel with the corresponding 10-km pixel. Despite SDEN has a lower range of variability than SD or SCA, and, probably, by using a more detailed resolution for SDEN we would obtain similar results. Nevertheless, it could be interesting to develop a methodology to estimate SDEN at the same resolution, although the very limited amount of SDEN data in Sierra Nevada made it unfeasible.

- We estimated SCA of MODIS in cloudy days by linear interpolation between the nearest previous and subsequent cloudless days. Although this approximation is good enough when the number of cloudy days is small, as in Sierra Nevada (Collados-Lara et al., 2017), it cannot be accurate enough for other mountain ranges, where more elaborated physically based methods to interpolate the SCA would be required (Molotch et al., 2004).

- SD is estimated by using a regression model without approaching any physical process. It is intended to be a parsimonious approach that may complement physical-based methodologies.

- The methodology is applicable to any mountain range. In this work, we focused on a single case study, Sierra Nevada Mountain, but future research works could analyse other mountain ranges.

- The approach is also useful to assess climate changes impacts on SWE through the modification of the non-steady variables. This research line is open for future works.

6. Conclusions

In this work we proposed a general method to estimate spatially distributed daily fields of SWE in a mountain range. This methodology provides useful information to analyse water resources planning and management alternatives and to assess climate change impacts in alpine systems (Goals 6 and 13 in the 2030 Agenda for Sustainable Development, adopted by all United Nations Member States in 2015).The approach is also useful when limited snow information is available. The proposed solution allows to study the historical dynamic of the snow in the mountain range, analyzing snow distribution for different snow seasons, duration of the snow seasons, number of accumulation and melting days, and distribution of SWE by elevation ranges. The approach, which combines a dynamic regression model of SD, SCA satellite data and simulations of SDEN, has been tested in Sierra Nevada (Southern Spain) and has been proved to be efficient to estimate SWE for the whole mountain range when limited information is available. The non-steady variables included in the dynamic regression model also allow to propagate impacts of climate change on SWE. For the case study the R^2 of the SD simulations obtained with the regression model defined with only steady variables is 0.59. When non-steady variables are incorporated the accuracy of the model is improved (R^2 0.64). In elevations below 1400 m a.s.l. the mean simulated SD value during the snow season (October to May) is not negligible, being higher than 35 cm for elevation higher than 2200 m a.s.l. Mean SDEN increases rapidly from around 100 kg m^{-3} at the beginning of the snow season to 500 kg m^{-3} at the end of the snow season without significant differences between elevation ranges. Note that melting events occurs even in winter and probably the snow mantle in Sierra Nevada is mostly isothermal. The mean total SWE accumulated in a snow season is around 330 Hm^3 and the maximum near to 480 Hm^3, being these resources very important for the region from the point of view of human consumption, tourism and ecosystems.

References

Alonso-González, E., López-Moreno, J. I., Gascoin, S., García-Valdecasas Ojeda, M., Sanmiguel-Vallelado, A., Navarro-Serrano, F., Revuelto, J., Ceballos, A., Esteban Parra, M. J., Essery, R. 2018. Daily gridded datasets of snow depth and snow water equivalent for the Iberian Peninsula from 1980 to 2014. Earth Syst. Sci. Data, 10, 303–315. https://doi.org/10.5194/essd-10-303-2018

Bavera, D., Bavay, M., Jonas, T., Lehning, M., De Michele, C. 2014. A comparison between two statistical and a physically-based model in snow water equivalent mapping. Advances in Water Resources, 63, 167-178. https://doi.org/10.1016/j.advwatres.2013.11.011

Brun, E., Vionnet, V., Boone, A., Decharme, B., Peings, Y., Valette, R., Karbou, F., Morin, S. 2013. Simulation of Northern Eurasian Local Snow Depth, Mass, and Density Using a Detailed Snowpack Model and Meteorological Reanalyses. J. Hydrometeor., 14, 203–219. https://doi.org/10.1175/JHM-D-12-012.1

Bormann, K. J., Westra, S., Evans, J. P., McCabe, M. F. 2013. Spatial and temporal variability in seasonal snow density. Journal of Hydrology, 484, 63-73. https://doi.org/10.1016/j.jhydrol.2013.01.032.

Carroll, S. S., Cressie, N. 1996. A comparison of geostatistical methodologies used to estimate snow water equivalent. Journal of the American Water Resources Association, 32, 267-278. https://doi.org/10.1111/j.1752-1688.1996.tb03450.x

Collados-Lara, A. J., Pardo-Iguzquiza, E., Pulido-Velazquez, D. 2017. Spatio-temporal estimation of snowpack thickness using point data from snow stakes, digital terrain models and satellite data. Hydrological Processes, 31, 1966–1982. https://doi.org/10.1002/hyp.11165

Collados-Lara, A. J., Pardo-Igúzquiza, E., Pulido-Velazquez, D., Jiménez-Sánchez, J. 2018. Precipitation fields in an alpine Mediterranean catchment. Inversion of precipitation gradient with elevation or undercatch of snowfall?. International Journal of Climatology, 38(9), 3565–3578. https://doi.org/10.1002/joc.5517

Collados-Lara, A. J., Pardo-Igúzquiza, E., Pulido-Velazquez, D. 2019. A distributed cellular automata model to simulate potential future impacts of climate change on snow cover area. Adv. Water Resour., 124, 106–119. https://doi.org/10.1016/j.advwatres.2018.12.010

Collados-Lara, A. J., Pardo-Igúzquiza, E., Pulido-Velazquez, D. 2020. Optimal design of snow stake networks to estimate snow depth in an alpine mountain range. Hydrological Processes, 34, 82–95. https://doi.org/10.1002/hyp.13574

Delgado-Ramos, F., Hervás-Gámez, C. 2018. Simple and Low-Cost Procedure for Monthly and Yearly Streamflow Forecasts during the Current Hydrological Year. Water, 10, 1038. https://doi.org/10.3390/w10081038

Dong, J., Walker, J. P., Houser, P. R. 2005. Factors affecting remotely sensed snow water equivalent uncertainty. Remote Sensing of Environment, 97(1), 68-82. https://doi.org/10.1016/j.rse.2005.04.010

Essery, R. 2015. A factorial snowpack model (FSM 1.0). Geosci. Model Dev., 8, 3867–3876. https://doi.org/10.5194/gmd-8-3867-2015

Fassnacht, S. R., Dressler, K. A., Bales, R. C. 2003. Snow water equivalent interpolation for the Colorado River basin from snow telemetry (SNOTEL) data. Water Resources Research, 39(8), 1208. https://doi.org/10.1029/2002WR001512 2003.

Fassnacht, S. R., Lopez-Moreno, J. I., Toro, M., Hultstrand, D. M. 2013. Mapping snow cover and snow depth across the Lake Limnopolar watershed on Byers Peninsula, Livingston Island, Maritime Antarctica. Antarctic Science, 252, 157–166. https://doi.org/10.1017/S0954102012001216

Fassnacht, S. R., López-Moreno, J. I., Ma, C., Weber, A. N., Pfohl, A. K. D., Kampf, S. K., Kappas, M. 2017. Spatio-temporal Snowmelt Variability across the Headwaters of the Southern Rocky Mountains. Frontiers of Earth Science, 11, 505–514. https://doi.org/10.1007/s11707-017-0641-4

Fassnacht, S. R., Venable, N. B., McGrath, D., Patterson, G. G. 2018. Sub-Seasonal Snowpack Trends in the Rocky Mountain National Park Area, Colorado, USA. Water, 10, 562. https://doi.org/10.3390/w10050562

Ferraro, R., Weng, F., Grody, N., Guch, I., Dean, C., Kongoli, C., Meng, H., Pellegrino, P., Zhao, L. 2002. NOAA satellite-derived hydrological products prove their worth. EOS Trans. Amer. Geophys. Union, 83, 429-437. https://doi.org/10.1029/2002EO000308

Ferraro, R. R., Weng, F., Grody, N. C., Zhao, L., Meng, H., Kongoli, C., Pellegrino, P., Qiu, S., Dean, C. 2005. NOAA operational hydrological products derived from the Advanced Microwave Sounding Unit. IEEE Trans. Geosci. Remote Sens., 43, 1036–1049. https://doi.org/10.1109/TGRS.2004.843249

García-Valdecasas Ojeda, M., Gámiz-Fortis, S. R., Castro-Díez, Y., Esteban-Parra, M. J. 2017. Evaluation of WRF capability to detect dry and wet periods in Spain using drought indices. J. Geophys. Res. Atmos., 122, 1569–1594, https://doi.org/10.1002/2016JD025683.

Gascoin, S., Hagolle, O., Huc, M., Jarlan, L., Dejoux, J. -F., Szczypta, C., Marti, R., Sánchez, R. 2015. A snow cover climatology for the Pyrenees from MODIS snow products. Hydrol. Earth Syst. Sci., 19, 2337–2351. https://doi.org/10.5194/hess-19-2337-2015

Gascoin, S., Grizonnet, M., Klempka, T., Salgues, G. 2018. Algorithm theoretical basis documentation for an operational snow cover product from Sentinel-2 and Landsat-8 data (Let-it-snow). https://doi.org/10.5281/zenodo.1414452

Girona-Mata, M., Miles, E. S., Ragettli, S., Pellicciotti, F. 2019. High-resolution snowline delineation from Landsat imagery to infer snow cover controls in a Himalayan catchment. Water Resources Research, 55, 6754– 6772. https://doi.org/10.1029/2019WR024935

Hall, D. K., Riggs, G. A., Salomonson, V. V., DiGirolamo, N. E., Bayr, K. J. 2002. MODIS snow-cover products. Remote Sens. Environ. 83, 181–194. https://doi.org/10.1016/S0034-4257(02)00095-0

Harpold, A. A., Guo, Q., Molotch, N, Brooks, P. D., Bales, R., Fernandez-Diaz, J. C., Musselman, K. N., Swetnam, T. L., Kirchner, P., Meadows, M. W., Flanagan, J., Lucas, R. . 2014. LiDAR-derived snowpack data sets from mixed conifer forests across the Western United States. Water Resources Research 50(3), 2749-2755. https://doi.org/10.1002/2013WR013935

Herrera, S., Fernández, J., Gutiérrez, J. M. 2016. Update of the Spain02 gridded observa- tional dataset for Euro-CORDEX evaluation: assessing the effect of the interpolation methodology. Int. J. Climatol., 36, 900–908. https://doi.org/10.1002/joc.4391

Herrero, J., Polo, M. J., Moñino, A., Losada, M. A. 2009. An energy balance snowmelt model in a Mediterranean site. J. Hydrol., 371, 98–107. https://doi.org/10.1016/j.jhydrol.2009.03.021

Herrero, J., Polo, M. J., Losada, M. A. 2011. Snow evolution in Sierra Nevada (Spain) from an energy balance model validated with Landsat TM data. In Proc. SPIE 8174, Remote Sensing for Agriculture, Ecosystems, and Hydrology XIII, 817403 (October 06, 2011)(pp. 817403-817403). https://doi.org/10.1117/12.898270

Jimeno-Sáez, P., Pulido-Velazquez, D., Collados-Lara, A. -J., Pardo-Igúzquiza, E., Senent-Aparicio, J., Baena-Ruiz, L. 2020. A Preliminary Assessment of the “Undercatching” and the Precipitation Pattern in an Alpine Basin. Water, 12, 1061. https://doi.org/10.3390/w12041061

Kuriqi, A., Pinheiro, A. N., Sordo-Ward, A., Garrote, L. 2019. Flow regime aspects in determining environmental flows and maximising energy production at run-of river hydropower plants. Appl Energy, 256, 113980. https://doi.org/10.1016/j.apenergy.2019.113980.

Langlois, A., Kohn, J., Royer, A., Cliche, P., Brucker, L., Picard, G., Fily, M., Derksen, C., Willemet, J. M. 2009. Simulation of Snow Water Equivalent (SWE) Using Thermodynamic Snow Models in Québec, Canada. J. Hydrometeor., 10, 1447–1463. https://doi.org/10.1175/2009JHM1154.1

Liston, G. E., Elder, K. 2006. A Distributed Snow-Evolution Modeling System (SnowModel). J. Hydrometeor., 7, 1259–1276. https://doi.org/10.1175/JHM548.1

Löffler, J. 2007. The influence of micro-climate, snow cover, and soil moisture on ecosystem functioning in high mountains. Journal of Geographical Sciences, 17, 3–19. https://doi.org/10.1007/s11442-007-0003-3

López-Moreno, J. I., Nogués-Bravo, D. 2006. Interpolating local snow depth data: an evaluation of methods. Hydrol. Process., 20, 2217-2232. https://doi.org/10.1002/hyp.6199

López-Moreno, J. I., Fassnacht, S., Latron, J., Musselman, K., Morán-Tejeda, E., Jonas, T. 2013. Small scale spatial variability of snow density and depth over complex alpine terrain: implications for estimating snow water equivalent. Advances in Water Research, 55, 40-52. https://doi.org/10.1016/j.advwatres.2012.08.010

Luojus, K., Pulliainen, J., Takala, M., Lemmetyinen, J. 2010. Snow Water Equivalent (SWE) product guide, European Space Agency Study Contract Report, ESRIN Contract 21703/08/I-EC.

Mankin, J., Viviroli, D., Singh, D., Hoekstra, A., Diffenbaugh, N. 2015. The potential for snow to supply human water demand in the present and future. Environmental Research Letters, 10, 114016. https://doi.org/10.1088/1748-9326/10/11/114016.

Marty, C., Tilg, A., Jonas, T. 2017. Recent Evidence of Large-Scale Receding Snow Water Equivalents in the European Alps. J. Hydrometeor., 18, 1021–1031. https://doi.org/10.1175/JHM-D-16-0188.1

Metsämäki, S., Pulliainen, J., Salminen, M., Luojus, K.,Wiesmann, A., Solberg, R., Böttcher, K., Hiltunen, M., Ripper, E. 2015. Introduction to GlobSnow Snow Extent products with considerations for accuracy assessment, Remote Sens. Environ., 156, 96–108. https://doi.org/10.1016/j.rse.2014.09.018

Mir, R. A., Jain, S. K., Saraf, A. K., Goswami, A. 2015. Accuracy assessment and trend analysis of MODIS-derived data on snow-covered areas in the Sutlej basin, Western Himalayas. International Journal of Remote Sensing, 36(15), 3837–3858. https://doi.org/10.1080/01431161.2015.1070320

Molotch, N. P., Colee, M. T., Bales, R. C., Dozier, J. 2005. Estimating the spatial distribution of snow water equivalent in an alpine basin using binary regression tree models: the impact of digital elevation data and independent variable selection. Hydrol. Process., 19, 1459-1479. https://doi.org/10.1002/hyp.5586

Molotch, N. P., Fassnacht, S. R., Bales, R. C., Helfrich, S. R. 2004. Estimating the distribution of snow water equivalent and snow extent beneath cloud cover in the salt–Verde River basin, Arizona. Hydrological Processes, 18(9), 1595–1611. https://doi.org/10.1002/hyp.1408

Natural Resources Conservation Service. 2016. NRCS: National Water and Climate Center SNOTEL data network. U.S. Department of Agriculture, available at: https://www.wcc.nrcs.usda.gov/snow/

Painter, T. H., Berisford, D. F., Boardman, J. W., Bormann, K. J., Deems, J. S., Gehrke, F., et al. 2016. The airborne snow observatory: Fusion of scanning lidar, imaging spectrometer, and physically-based modeling for mapping snow water equivalent and snow albedo. Remote Sensing of Environment, 184, 139–152. https://doi.org/10.1016/j.rse.2016.06.018

Pardo-Iguzquiza, E., Collados-Lara, A. J., Pulido-Velazquez, D. 2017. Estimation of the spatiotemporal dynamics of snow covered area by using cellular automata models. J. Hydrol., 550, 230–238. https://doi.org/10.1016/j.jhydrol.2017.04.058 .

Pimentel, R., Herrero, J., Polo, M. J. 2017. Snow Cover Fraction (SCF) and snow depth obtained using terrestrial photography (2009-2013) in the control area Refugio Poqueira (Sierra Nevada, Spain). PANGAEA. https://doi.org/10.1594/PANGAEA.871706.

Prusova, M., Orlikova, L., Hanzlova, M. 2012. Comparison of geostatistical approaches dealing with the distribution of snow. cent.eur.j.geo. 4, 603–613. https://doi.org/10.2478/s13533-012-0103-1

Ren, W., Yang, T., Shi, P., Xu, C. -Y., Zhang, K., Zhou, X., Shao, Q., Ciais, P. 2018. A probabilistic method for streamflow projection and associated uncertainty analysis in a data sparse alpine region. Glob. Planet. Chang., 165, 100–113. https://doi.org/10.1016/j.gloplacha.2018.03.011

Richer, E. E., Kampf, S. K., Fassnacht, S. R., Moore, C. C. 2013. Spatiotemporal index for analyzing controls on snow climatology: Application in the Colorado front range. Physical Geography, 342, 85–107. https://doi.org/10.1080/02723646.2013.787578

Rosenberg, E. A., Wood, A. W., Steinemann, A. C. 2011. Statistical applications of physically based hydrologic models to seasonal streamflow forecasts. Water Resour. Res., 47, W00H14. https://doi.org/10.1029/2010WR010101.

Sanmiguel-Vallelado, A., Morán-Tejeda, E., Alonso-González, E. et al. 2017. Effect of snow on mountain river regimes: an example from the Pyrenees. Front. Earth Sci., 11, 515–530. https://doi.org/10.1007/s11707-016-0630-z

Salomonson, V.V., Appel, I. 2004. Estimating fractional snow cover from MODIS using the normalized difference snow index. Remote Sensing of Environment, 89(3), 351-360. https://doi.org/10.1016/j.rse.2003.10.016.

Shaw, T. E., Gascoin, S., Mendoza, P. A., Pellicciotti, F., McPhee, J. 2020. Snow depth patterns in a high mountain andean catchment from satellite optical tristereoscopic remote sensing. Water Resources Research, 56, e2019WR024880. https://doi.org/10.1029/2019WR024880

Skamarock, W. C., Klemp, J. B., Dudhia, J., Gill, D. O., Barker, D., Duda, M. G., Powers, J. G. 2008. A Description of the Advanced Research WRF Version 3 (No. NCAR/TN-475+STR). University Corporation for Atmospheric Research. https://doi.org/10.5065/D68S4MVH

Skaugen, T., Melvold, K. 2019. Modeling the snow depth variability with a high-resolution lidar data set and nonlinear terrain dependency. Water Resources Research, 55, 9689– 9704. https://doi.org/10.1029/2019WR025030

Soboll, A., Dingeldey, A. 2012. The future impact of climate change on Alpine winter tourism: a high-resolution simulation system in the German and Austrian Alps. Journal of Sustainable Tourism, 20(1), 101-120. https://doi.org/10.1080/09669582.2011.610895

Sturm, M., Goldstein, M. A., Parr, C. 2017. Water and life from snow: A trillion dollar science question. Water Resour. Res., 53, 3534– 3544. https://doi.org/10.1002/2017WR020840.

Verseghy, D. L. 1991. Class—A Canadian land surface scheme for GCMS. I. Soil model. Int. J. Climatol., 11,111-133. https://doi.org/10.1002/joc.3370110202

Viviroli, D., Archer, D. R., Buytaert, W., Fowler, H. J., Greenwood, G. B., Hamlet, A. F., Huang, Y., Koboltschnig, G., Litaor, M. I., López-Moreno, J. I., Lorentz, S., Schädler, B., Schreier, H., Schwaiger, K., Vuille, M., Woods, R. 2011. Climate change and mountain water resources: overview and recommendations for research, management and policy. Hydrology and Earth System Sciences, 15(2), 471-504. https://doi.org/10.5194/hess-15-471-2011

Wrzesien, M. L., Durand, M. T., Pavelsky, T. M., Howat, I. M., Margulis, S. A., Huning, L. S. 2017. Comparison of Methods to Estimate Snow Water Equivalent at the Mountain Range Scale: A Case Study of the California Sierra Nevada. J. Hydrometeor., 18, 1101–1119. https://doi.org/10.1175/JHM-D-16-0246.1

Zappa, M., Holko, L., Šanda, M., Vitvar, T., Parajka, J. 2019. Thematic Issue on Snow Resources and Hydrological Cycle. J. Hydrol. Hydromech., 67, 1, 1–3. https://doi.org/10.2478/johh-2018-0027

Zeinivand, H., De Smedt, F. 2009. Simulation of snow covers area by a physical based model. World Academy of Science, Engineering and Technology, 55, 469–474. https://doi.org/10.5281/zenodo.1055118

Zhang, F., Zhang, H., Hagen, S. C., Ye, M., Wang, D., Gui, D., Zeng, C., Tian, L., Liu, J. 2014. Snow cover and runoff modelling in a high mountain catchment with scarce data: effects of temperature and precipitation parameters. Hydrol. Process., 29, 52–65. https://doi.org/10.1002/hyp.10125

Acknowledgements

This research has been partially supported by the SIGLO-AN project (RTI2018-101397-B-I00) from the Spanish Ministry of Science, Innovation and Universities (Programa Estatal de I+D+I orientada a los Retos de la Sociedad). We would also like to thank the ERHIN program, the NASA DAAC and Pimentel et al. (2017) for the data provided for this study.

Model name	Model structure	Temporal accumulation non-steady variable	Non-steady variable	Condition to accumulate
m1_v1_SCA	$Y_1 = \beta_0 + (\beta_1 x_i + \beta_2 x_j + \beta_3 x_\ell x_k) t_n$	$t^1_{v,\zeta} = \frac{1}{2\zeta + 1} \sum_{v-\zeta}^{v+\zeta} t_w$	SCA	-
m1_v2_SCA	$Y_1 = \beta_0 + (\beta_1 x_i + \beta_2 x_j + \beta_3 x_\ell x_k) t_n$	$t^2_{v,\zeta} = \frac{1}{\zeta + 1} \sum_{v-\zeta}^{v} t_w$	SCA	-
m2_v1_SCA	$Y_2 = (\beta_0 + \beta_1 x_i + \beta_2 x_j + \beta_3 x_\ell x_k) t_n$	$t^1_{v,\zeta} = \frac{1}{2\zeta + 1} \sum_{v-\zeta}^{v+\zeta} t_w$	SCA	-
m2_v2_SCA	$Y_2 = (\beta_0 + \beta_1 x_i + \beta_2 x_j + \beta_3 x_\ell x_k) t_n$	$t^2_{v,\zeta} = \frac{1}{\zeta + 1} \sum_{v-\zeta}^{v} t_w$	SCA	-
m3_v1_SCA	$Y_3 = \beta_0 + \beta_1 x_i t_n + \beta_2 x_j t_o + \beta_3 x_\ell x_k t_p$	$t^1_{v,\zeta} = \frac{1}{2\zeta + 1} \sum_{v-\zeta}^{v+\zeta} t_w$	SCA	-
m3_v2_SCA	$Y_3 = \beta_0 + \beta_1 x_i t_n + \beta_2 x_j t_o + \beta_3 x_\ell x_k t_p$	$t^2_{v,\zeta} = \frac{1}{\zeta + 1} \sum_{v-\zeta}^{v} t_w$	SCA	-
m3_v1_P(Tmin)	$Y_3 = \beta_0 + \beta_1 x_i t_n + \beta_2 x_j t_o + \beta_3 x_\ell x_k t_p$	$t^1_{v,\zeta} = \frac{1}{2\zeta + 1} \sum_{v-\zeta}^{v+\zeta} t_w$	P	Min T<0
m3_v2_P(Tmin)	$Y_3 = \beta_0 + \beta_1 x_i t_n + \beta_2 x_j t_o + \beta_3 x_\ell x_k t_p$	$t^2_{v,\zeta} = \frac{1}{\zeta + 1} \sum_{v-\zeta}^{v} t_w$	P	Min T<0
m3_v1_P(Tmean)	$Y_3 = \beta_0 + \beta_1 x_i t_n + \beta_2 x_j t_o + \beta_3 x_\ell x_k t_p$	$t^1_{v,\zeta} = \frac{1}{2\zeta + 1} \sum_{v-\zeta}^{v+\zeta} t_w$	P	Mean T <0
m3_v2_P(Tmean)	$Y_3 = \beta_0 + \beta_1 x_i t_n + \beta_2 x_j t_o + \beta_3 x_\ell x_k t_p$	$t^2_{v,\zeta} = \frac{1}{\zeta + 1} \sum_{v-\zeta}^{v} t_w$	P	Mean T <0

Table 1. Considered models depending on the model structure, non-steady variable, and option of accumulation of the non-steady variable.

Model	R^2_{adj}	NLLF	AIC	BIC	KIC
Steady model	0.59	3534.06	7076.13	7094.17	7114.26
m3_v2_SCA ζ = 25	0.63	3491.90	6991.79	7009.84	7026.35
m3_v1_SCA ζ =30	0.63	3493.94	6995.89	7013.93	7029.80
m3_v2_P(Tmin) ζ =120	0.61	3509.74	7027.49	7045.53	7059.36

Table 2. Goodness of fit of the steady approach and three non-steady models expressed in terms of the adjusted R^2 (R^2_{adj}), the negative of the logarithm of likelihood function (NLLF), the Akaike information criterion (AIC), the Bayesian information criterion (BIC), and the Kashyap information criterion (KIC).

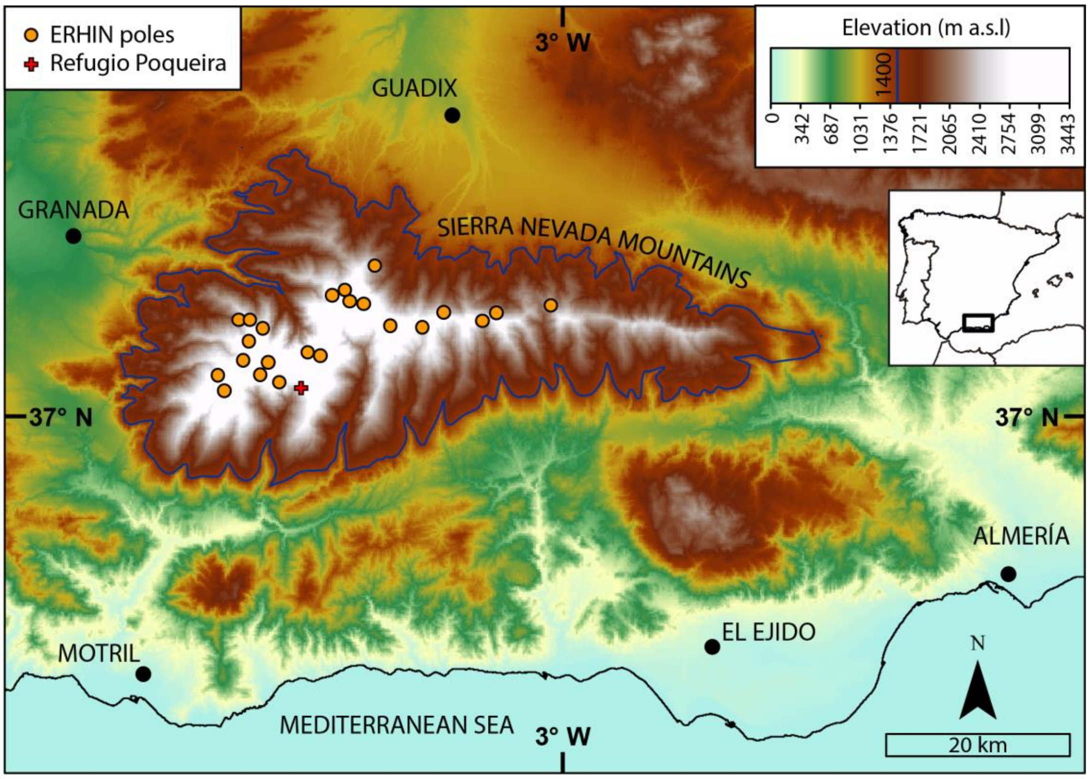

Figure 1. Location of the case study and SD measurements points (yellow dots) and snow data of the Poqueira site (red cross).

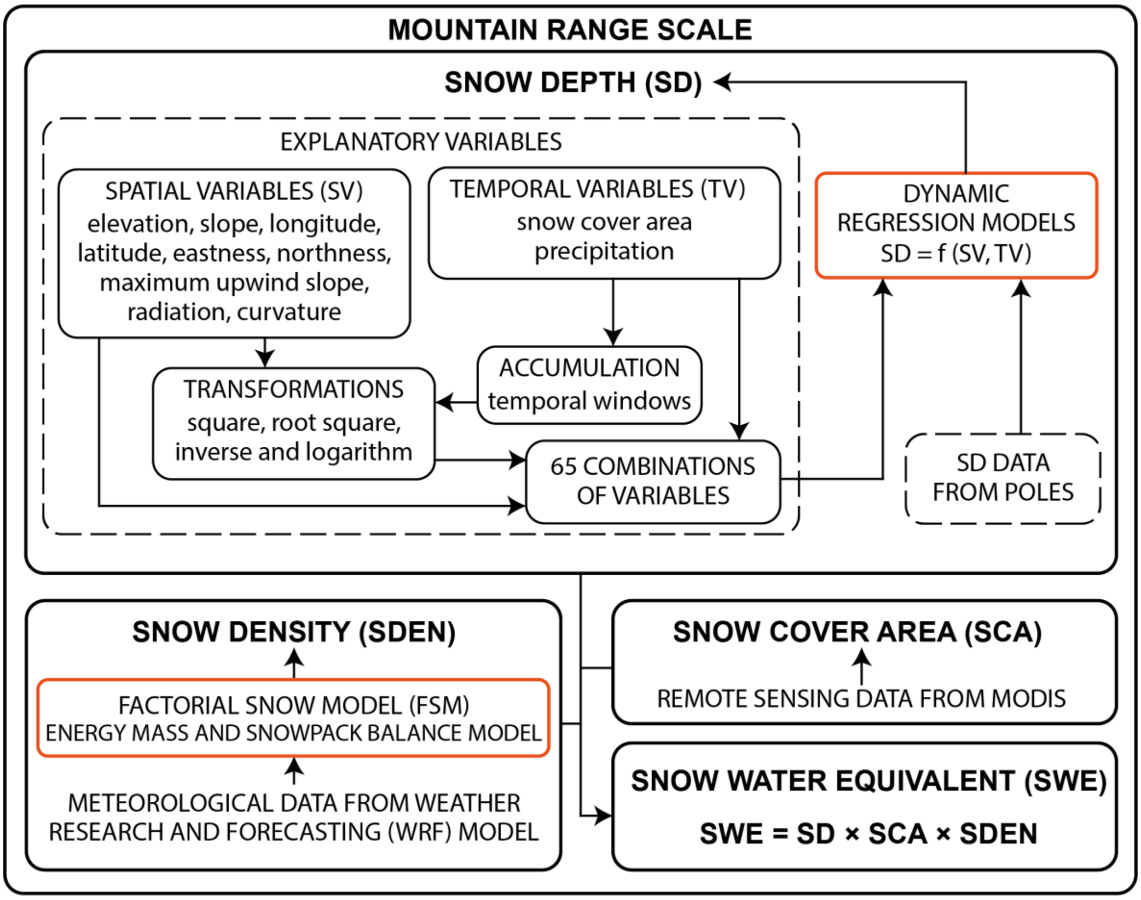

Figure 2. Flow chart of the proposed methodology to assess SWE in a mountain range.

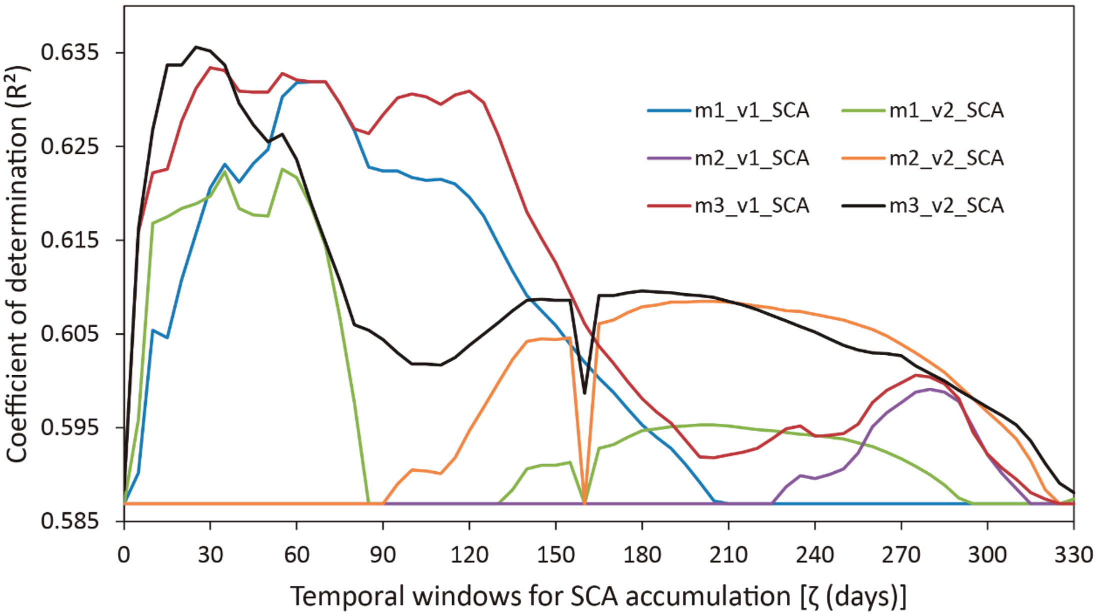

Figure 3. Coefficient of determination of the regression models using a SCA index (accumulated for different temporal windows) as non-steady explanatory variable.

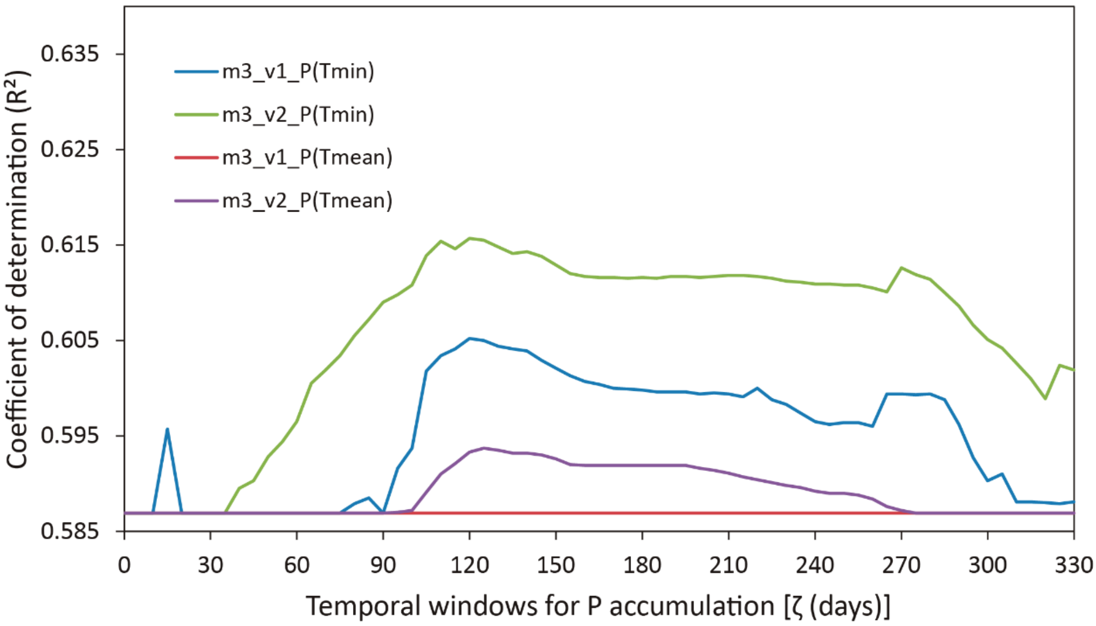

Figure 4. Coefficient of determination of the regression models using a P index (accumulated for different temporal windows) as non-steady explanatory variable.

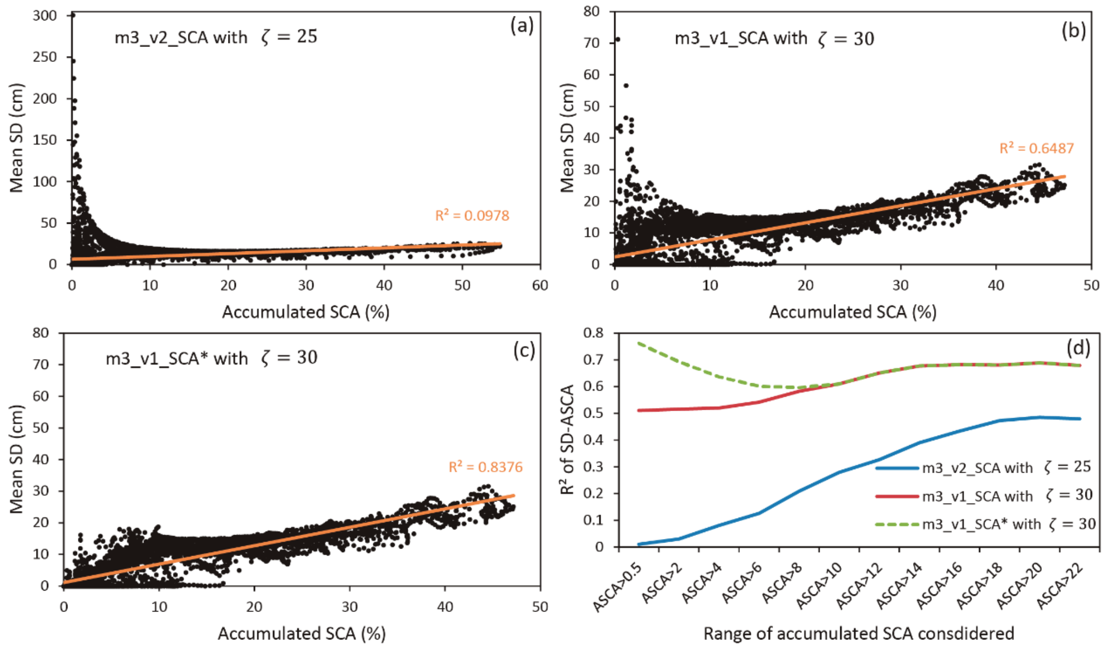

Figure 5. Relationship between mean SD and accumulated SCA (ASCA) using model m3, the structure of accumulation of SCA v2 and $\zeta = 25$ (a), using model m3, the structure of accumulation of SCA v1 and $\zeta = 30$, using model m3, the structure of accumulation of SCA v1 and $\zeta = 30$ when ASCA is higher than 10% and the steady model when ASCA is lower than 10% (c), and correlation coefficient for different thresholds of ASCA for the model structures of (a), (b), and (c).

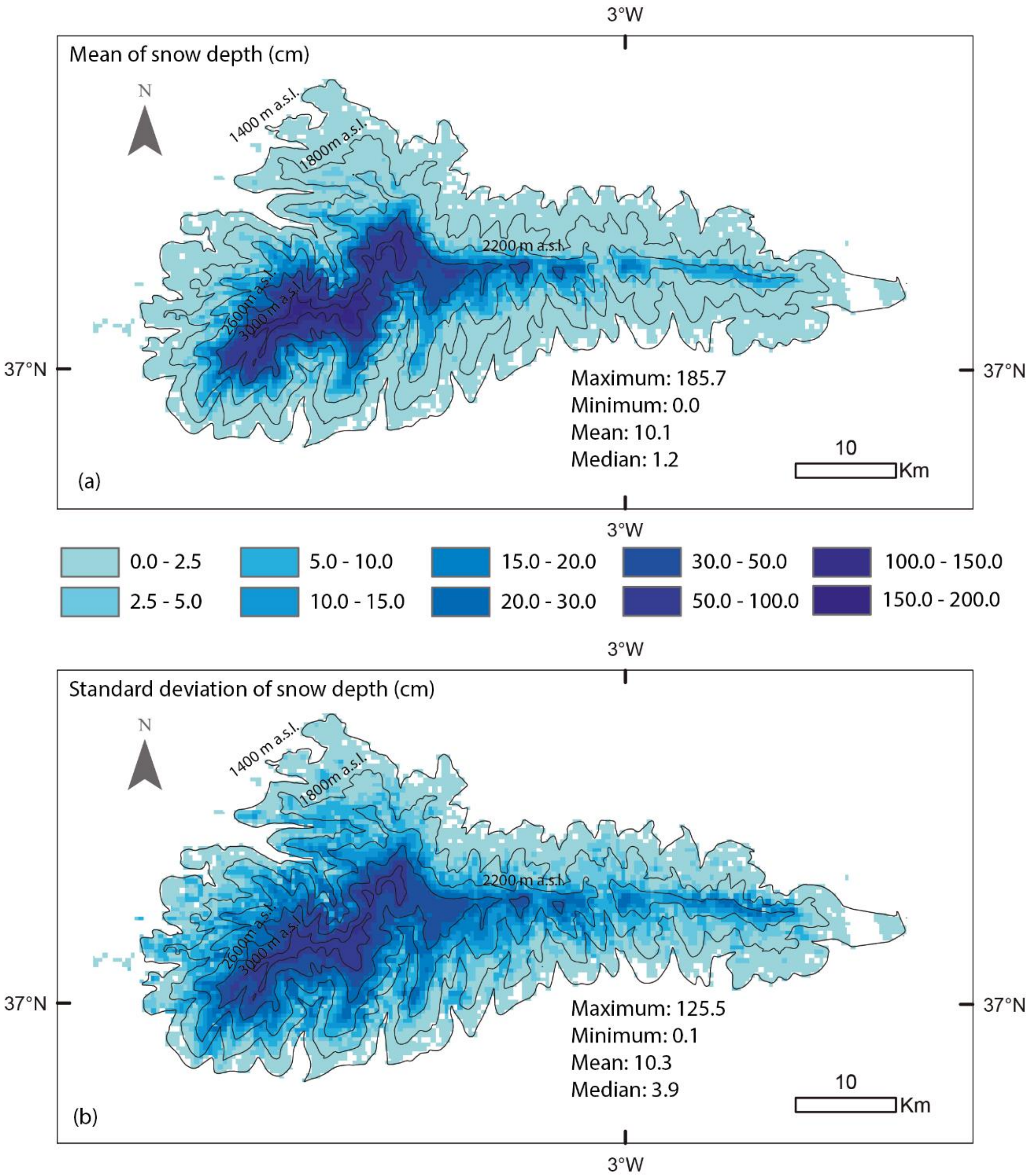

Figure 6. Maps of the spatial distribution of mean SD (a) and standard deviation of SD (b) for the snow season (October to May) in the period 2000–2015.

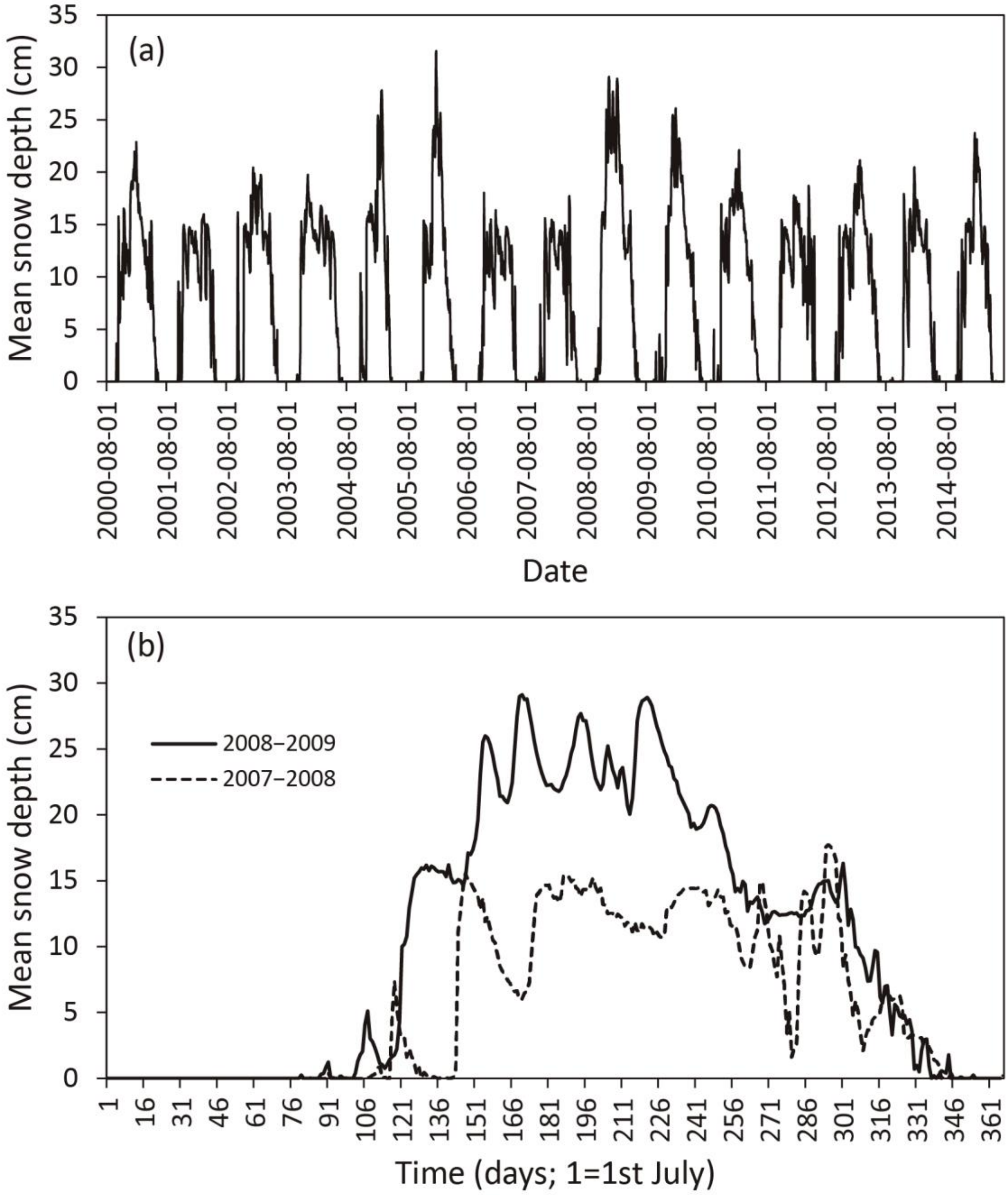

Figure 7. Temporal series of mean daily SD in the mountain range: for the period 2000−2015 (a) and for the snow season 2007−2008 (season with the smallest accumulation of snow) and 2008−2009 (season with the largest accumulation of snow) (b).

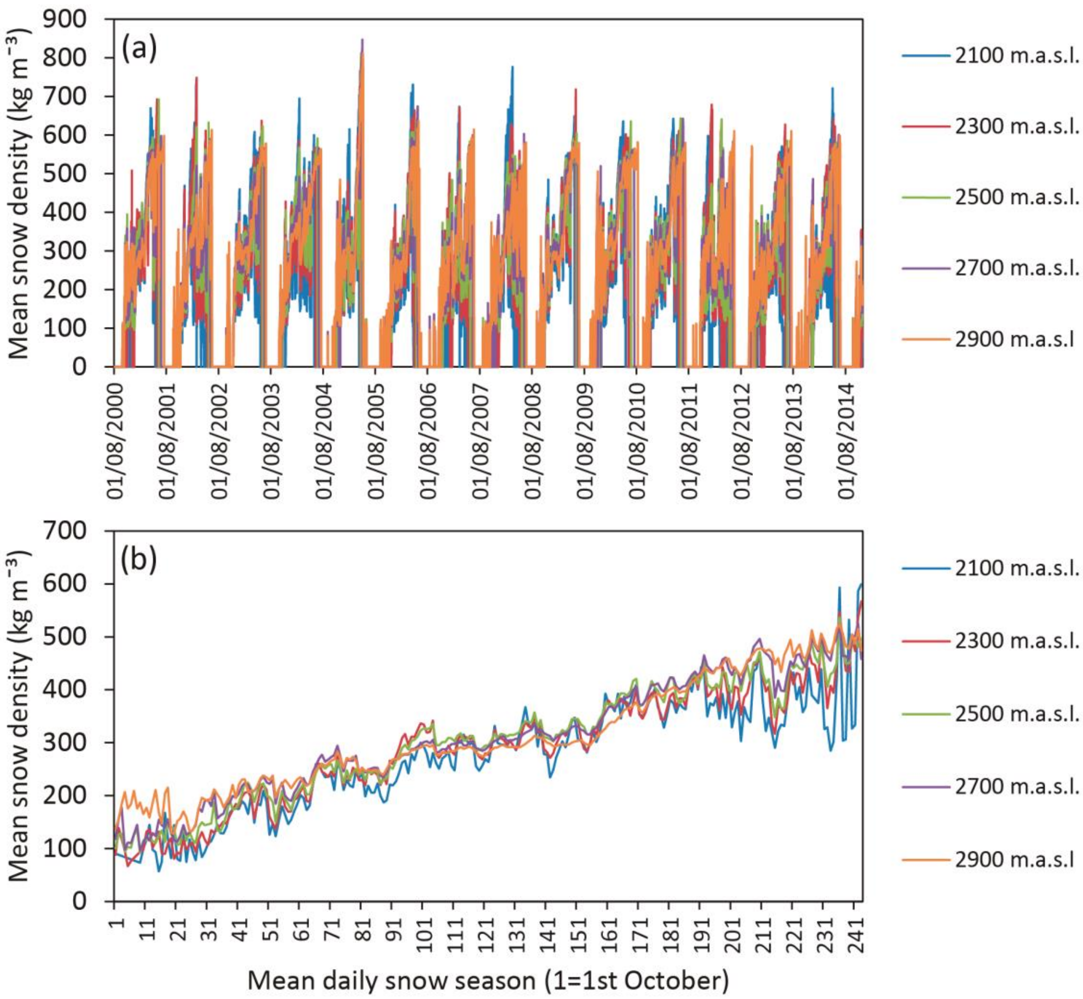

Figure 8. Temporal series of the mean daily SDEN in the mountain range for different elevations within the period 2000-2014 (a) and SDEN for the mean daily snow season.

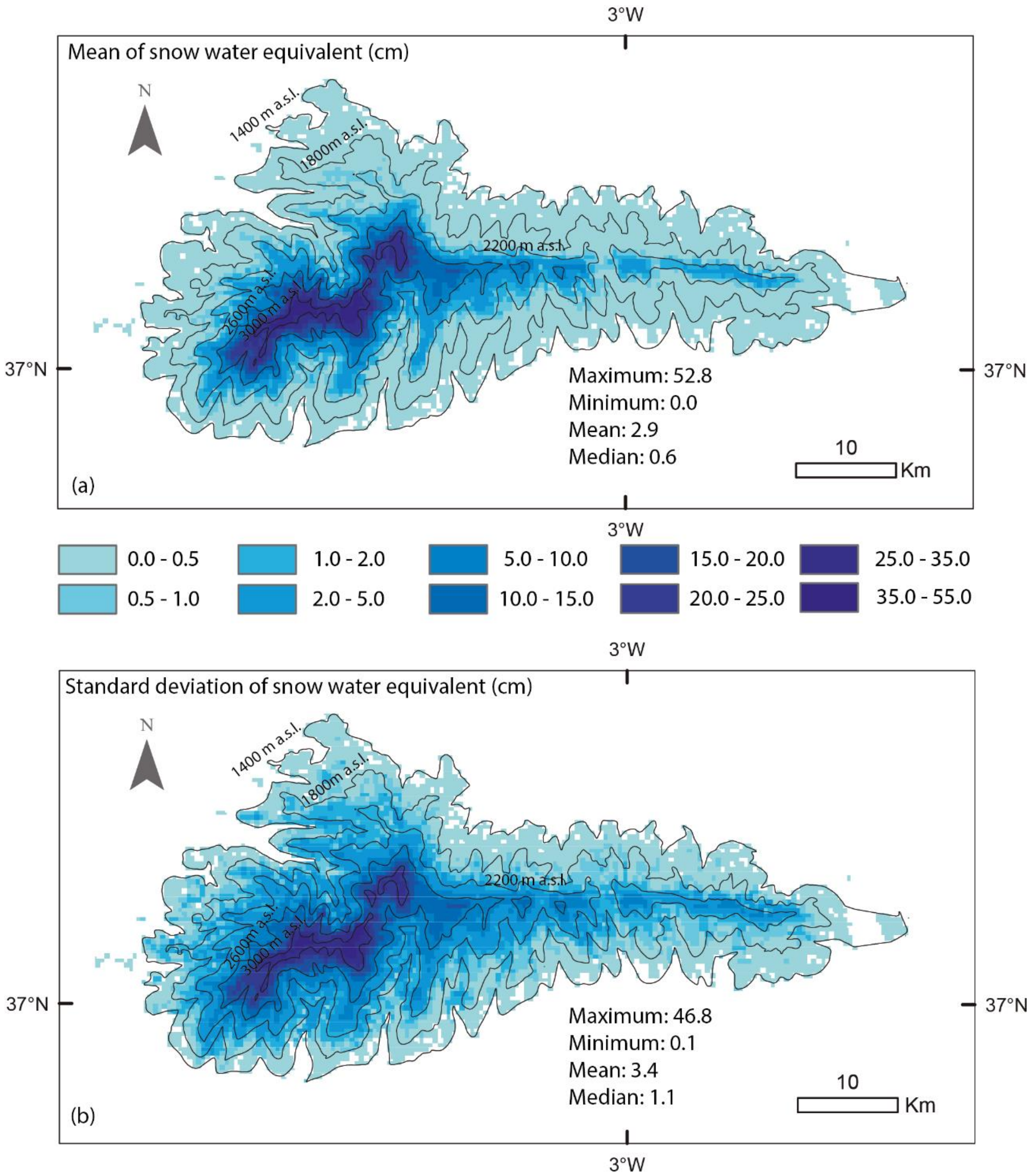

Figure 9. Maps of the spatial distribution of mean SWE (a) and standard deviation of SWE (b) for the snow season (October to May) in the period 2000–2014.

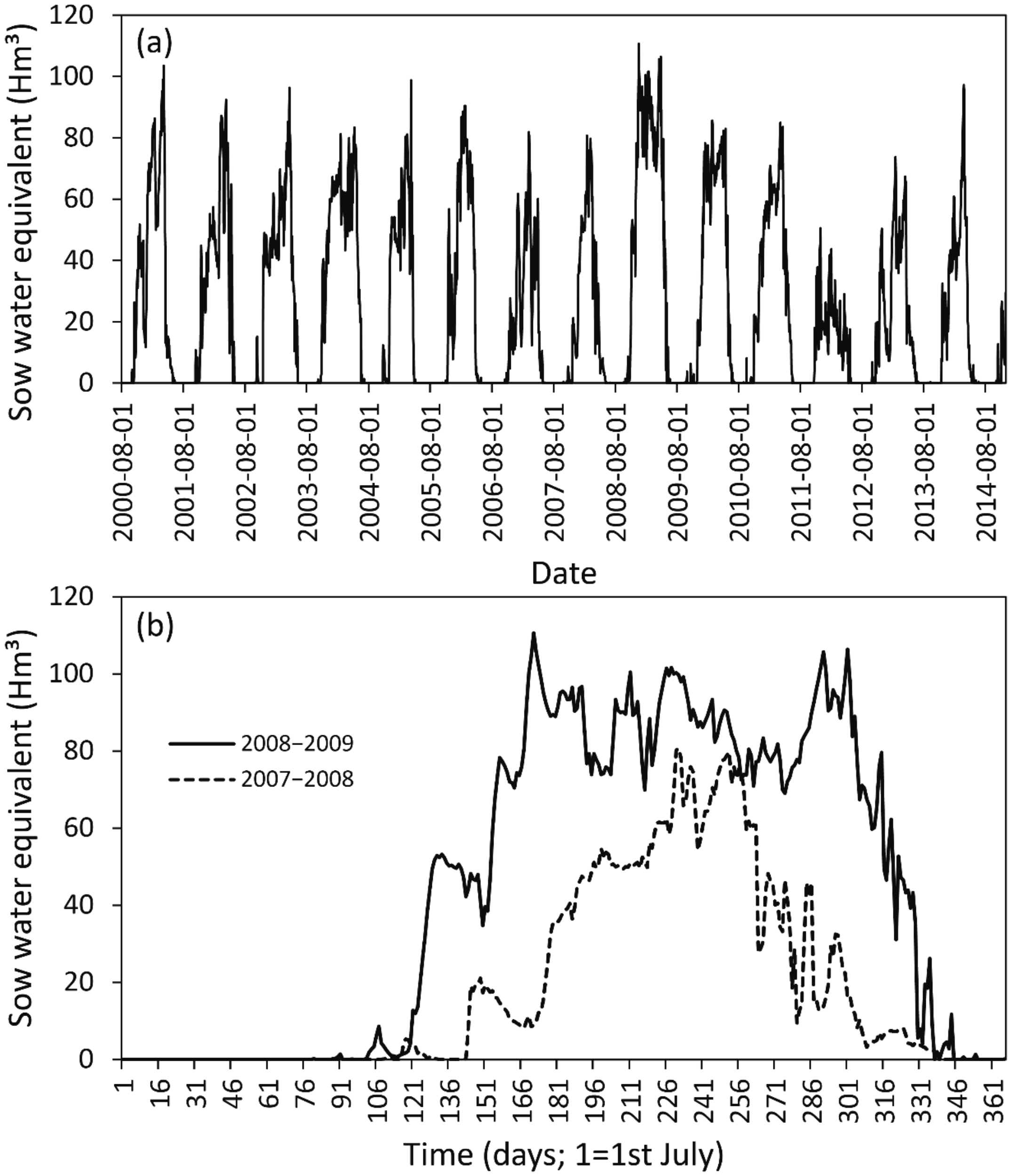

Figure 10. Temporal series of the SWE in the mountain range: for the period 2000−2014 (a) and for the snow season 2007−2008 (season with the smallest accumulation of snow) and 2008−2009 (season with the largest accumulation of snow) (b).

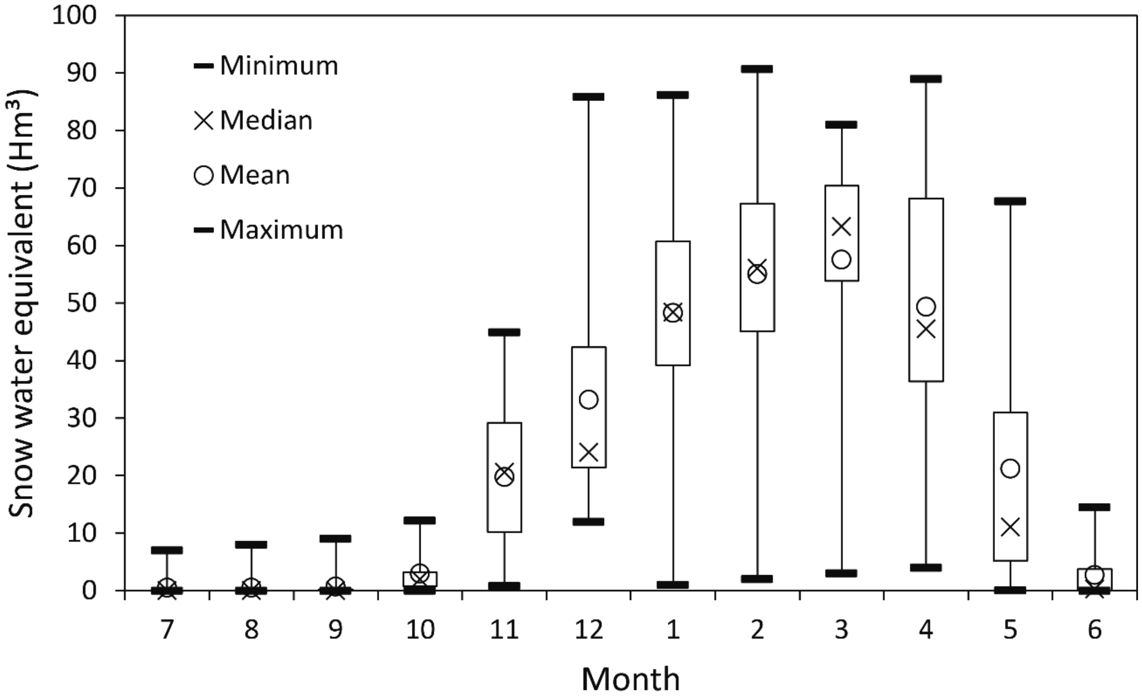

Figure 11. Mean year at monthly scale for the SWE in the mountain range.

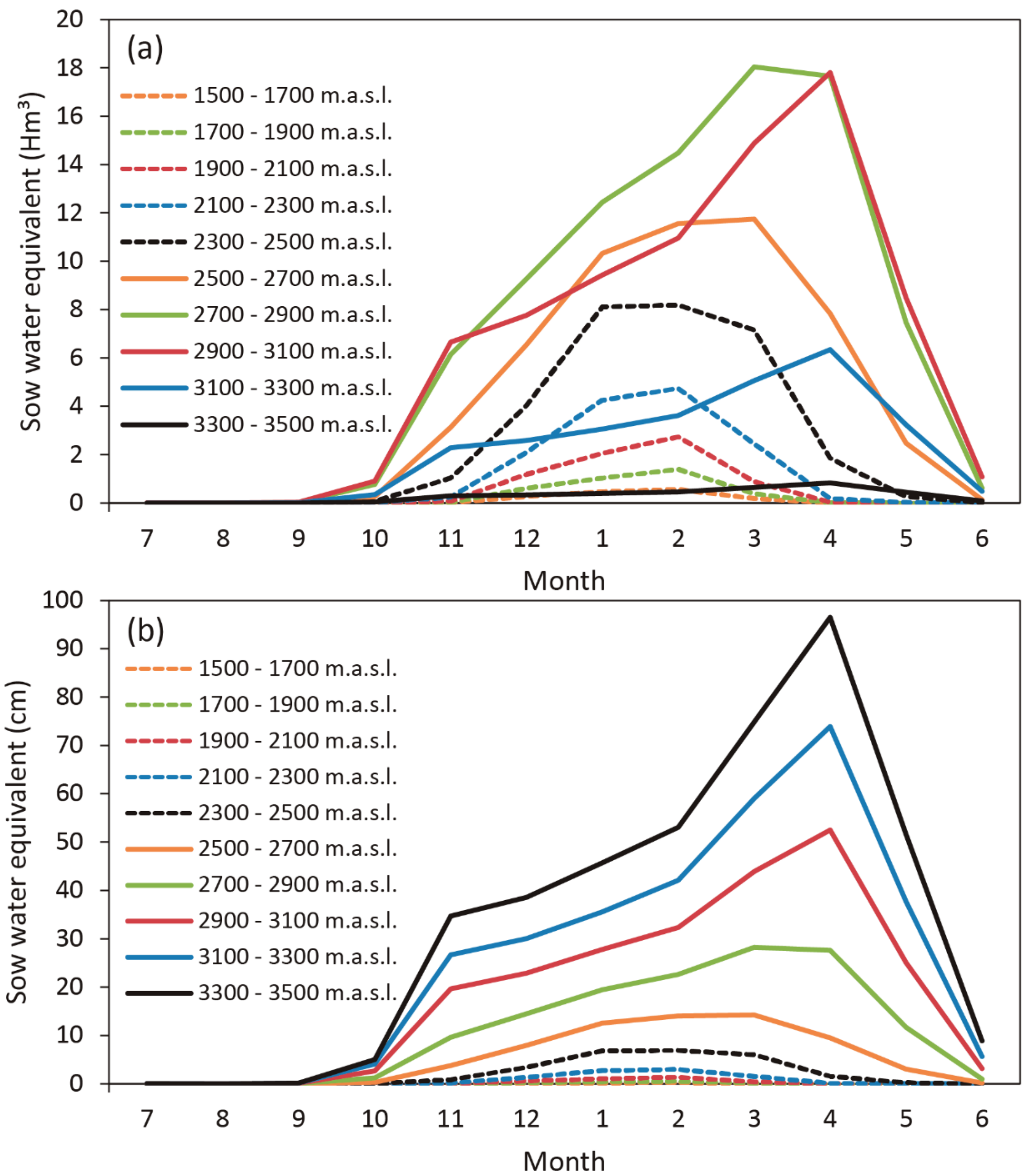

Figure 12. Mean year at monthly scale for the SWE in different elevation ranges measured in volume (a) and in depth of water (b).

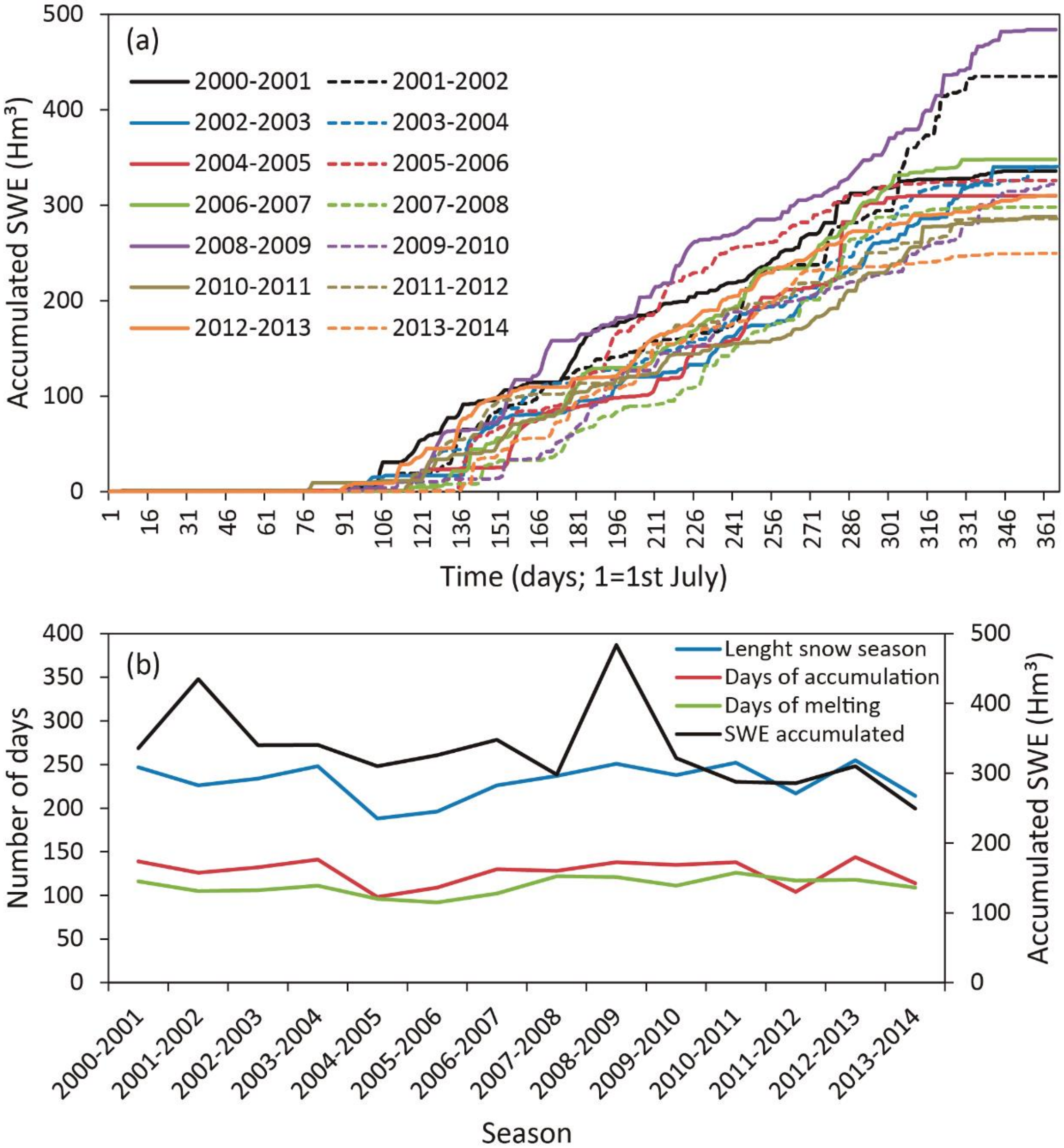

Figure 13. Temporal series of the accumulated SWE in the mountain range for different snow seasons (a) and snow period length, number of snow accumulation and melting days, and total SWE accumulated for each snow season (b).